Octave-spanning ultraflat supercontinuum with soft-glass photonic crystal fibers

J. J. Miret,[1,*] E. Silvestre,[2] and P. Andrés[2]

[1]*Departamento de Óptica, Universidad de Alicante, 08080 Alicante, Spain*
[2]*Departamento de Óptica, Universidad de Valencia, 46100 Burjassot, Spain*
[*]*Corresponding author: jjmiret@ua.es*

Abstract: We theoretically identify some photonic-crystal-fiber structures, made up of soft glass, that generate ultrawide (over an octave) and very smooth supercontinuum spectra when illuminated with femtosecond pulsed light. The design of the fiber geometry in order to reach a nearly ultraflattened normal dispersion behavior is crucial to accomplish the above goal. Our numerical simulations reveal that these supercontinuum sources show high stability and no significant changes are detected even for fairly large variations of the incident pulse.

OCIS codes: (190.4370) nonlinear optics, fibers; (190.5530) pulse propagation and temporal solitons; (320.2250) femtosecond phenomena

References and links

1. P. St. J. Russell, "Photonic-Crystal fibers," J. Lightwave Technol. **24,** 4729-4749 (2006).
2. D. Mogilevtsev, T. A. Birks, and P. St. J. Russell, "Group-velocity dispersion in photonic crystal fibers," Opt. Lett. **23,** 1162-1164 (1998).
3. A. Ferrando, E. Silvestre, J. J. Miret, and P. Andrés, "Nearly zero ultraflattened dispersion in photonic crystal fibers," Opt. Lett. **11,** 790-792 (2000).
4. A. Ferrando, E. Silvestre, P. Andrés, J. J. Miret, and M. V. Andrés, "Designing the properties of dispersion-flattened photonic crystal fibers," Opt. Express **9,** 687-697 (2001).
5. J. M. Dudley, G. Genty, and S. Coen, "Supercontinuum generation in photonic crystal fiber," Rev. Mod. Phys. **78,** 1135-1184 (2006).
6. J. K. Ranka, R. S. Windeler, and A. J. Stentz, "Visible continuum generation in air-silica microstructure optical fibers with anomalous dispersion at 800 nm," Opt. Lett. **25,** 25-27 (2000).
7. X. Gu, L. Xu, M. Kimmel, E. Zeek, P. O'Shea, A. P. Shreenath, R. Trebino, and R. S. Windeler, "Frequency-resolved optical gating and single-shot spectral measurements reveal fine structure in microstructure-fiber continuum," Opt. Lett. **27,** 1174-1176 (2002).
8. K. L. Corwin, N. R. Newbury, J. M. Dudley, S. Coen, S. A. Diddams, K. Weber, and R. S. Windeler, "Fundamental noise limitations to supercontinuum generation in microstructure fiber," Phys. Rev. Lett. **90**, 113904 (2003).
9. A. Unterhuber, B Považay, K. Bizheva, B. Hermann, H. Sattmann, A. Stingl, T. Le, M. Seefeld, R. Menzel, M. Preusser, H. Budka, Ch. Schubert, H. Reitsamer, P. K. Ahnelt, J. E. Morgan, A. Cowey, and W. Drexler, "Advances in broad bandwidth light sources for ultrahigh resolution optical coherence tomography," Phys. Med. Biol. **49**, 1235-1246 (2004).
10. T. Hori, J. Takayanagi, N. Nishizawa, and T. Goto, "Flatly broadened, wideband and low noise supercontinuum generation in highly nonlinear hybrid fiber," Opt. Express **12,** 317-324 (2004).
11. H. Ebendorff-Heidepriem and T. M. Monro, "Extrusion of complex preforms for microstructured optical fibers," Opt. Express **15,** 15086-15092 (2007).
12. J. Y. Y. Leong, P. Petro, J. H. V. Price, H. Ebendorff-Heidepriem, S. Asimakis, R. C. Moore, K. E. Frampton, V. Finazzi, X. Feng, T. M. Monro, and D. J. Richardson, "High-nonlinear dispersion-shifted lead-silicate holey fibers for efficient 1-μm pumped supercontinuum generation," J. Lightwave Technol. **24,** 183-190 (2006).
13. F. G. Omenetto, N. A. Wolchover, M. R. Wehner, M. Ross, A. Efimov, A. J. Taylor, V. V. R. K. Kumar, A. K. George, J. C. Knight, N. Y. Joly, and P. St. J. Russell, "Spectrally smooth supercontinuum from 350 nm to 3 μm in sub-centimeter lengths of soft-glass photonic crystal fibers," Opt. Express **14,** 4928-4934 (2006).
14. *Schoot E-Catalogue 2003 Optical Glass*, Schoot Glass, Mainz, Germany.
15. E. Silvestre, T. Pinheiro-Ortega, P. Andrés, J. J. Miret, and A. Ortigosa-Blanch, "Analytical evaluation of chromatic dispersion in photonic crystal fibers," Opt. Lett. **30,** 453-455 (2005).
16. E. Silvestre, T. Pinheiro-Ortega, P. Andrés, J. J. Miret, and A. Coves, "Differential toolbox to shape dispersion behavior in photonic crystal fibers," Opt. Lett. **31,** 1190-1192 (2006).

#107640 - $15.00 USD Received 18 Feb 2009; revised 3 Apr 2009; accepted 3 Apr 2009; published 15 May 2009

17. G. P. Agrawal, *Nonlinear Fiber Optics*, 3rd ed. (Academic Press, San Diego, CA, 2001).
18. V. L. Kalashnikow, E. Sorokin, and I. T. Sorokina, "Raman effects in the infrared supercontinuum generation in soft-glass PCFs," App. Phys. B **87,** 37-44 (2007).
19. W. J. Tomlinson, R. H. Stolen, and C. V. Shank, "Compression of optical pulses chirped by self-phase modulation in fibers," J. Opt. Soc. Amer. B **1,** 139-149 (1984).
20. N. A. Wolchover , F. Luan, A. K. George, J. C. Knight, and F. G. Omenetto, "High nonlinearity glass photonic crystal nanowires," Opt. Express **15**, 829-833 (2007).
21. A. Apolonski, B. Povazay, A. Unterhuber, W. Drexler, W. J. Wadsworth, J. C. Knight, and P. St. J. Russell, "Spectral shaping of supercontinuum in a cobweb photonic-crystal fiber with sub-20-fs pulses," J. Opt. Soc. Am. B **19**, 2165-2170 (2002).

1. Introduction

Photonic crystal fibers (PCFs) show a wide set of singular properties and, consequently, a plethora of new applications have been found in many areas of science and technology [1]. One of their most interesting features is the ability to engineer the group velocity dispersion (GVD). Generally speaking, the whole dispersion derives from the combination of material and waveguide contributions. On one hand, the material dispersion component is fixed by the fabrication material, usually fused silica. However the high refractive-index contrast between the fused silica and the air holes leads to a very strong waveguide-dispersion contribution that, in fact, is very sensitive to the geometric distribution of the air holes in the photonic crystal cladding. Therefore, if we manipulate the geometry of the PCF, we can obtain very uncommon dispersion profiles. In this way, some PCF configurations that shift the intrinsic zero-dispersion wavelength (ZDW) of silica well below 1.3 μm were reported [2], as well as other PCF structures showing ultraflattened dispersion profiles [3, 4].

In addition, supercontinuum (SC) generation based on PCFs is currently a cutting-edge photonics research [5]. SC provides a very attractive optical source for several applications, such as optical coherence tomography, ultrashort pulse generation, optical frequency metrology, etc. The conjunction of two unusual properties shown by PCFs, high modal confinement and ZDW's shift, has successfully allowed the achievement of ultrabroad SC spectra [5, 6]. Typically, SC generation in PCFs is realized by injecting the pump pulse into the anomalous dispersion region of the fiber, near the ZDW. The spectral broadening arises from the interplay among several nonlinear effects. In particular, soliton fission and Raman self-frequency shift are responsible for the long-wavelength component production, whereas dispersive wave generation originates the short-wavelength components. In this dispersion regime, the soliton fission process is strongly perturbed by nonlinear effects as the modulation instability (MI), higher-order dispersion terms, and Raman scattering, where the relative contribution of each one depends on pump pulse duration. The output is usually a SC spectrum showing significant spectral oscillations (around 20 dB), an unstable fine spectral structure, and low-coherence properties [7, 8], which in many cases limit its practical applications, as for example in OCT [9]. It also sets a fundamental limitation on the compression of ultrashort pulses. One way to avoid the above spectral fluctuations is to pump in the normal dispersion regime. This fact suppresses MI and soliton fission, and hence improves the coherence and spectral flatness, but with the drawback of a narrower spectral broadening [10].

Recent advances in the fabrication of soft-glass PCFs [11], i.e., PCFs made up of soft transparent materials that show a very high nonlinear-index coefficient, open new possibilities in SC generation. Up to now, the research work has focused its attention on the optimization of both the nonlinear response and the location of the ZDW [12]. Some results showed that soft-glass PCFs generate a very broad SC, covering a bandwidth greater than 2000 nm, when operating at the anomalous dispersion regime. In this case, the SC suffers from the same lack of spectral flatness [13], as in fused-silica PCFs. However, one can expect that operating at the normal dispersion regime, the coherence and spectral flatness be improved, and the high nonlinearity may also compensate, at least to some extent, the above-mentioned spectral bandwidth reduction.

#107640 - $15.00 USD Received 18 Feb 2009; revised 3 Apr 2009; accepted 3 Apr 2009; published 15 May 2009

The aim of this paper is twofold. First we recognize a soft-glass triangular PCF geometry that, as in fused-silica PCFs, shows ultraflattened normal dispersion over a wide wavelength interval around 1.55 μm. In a second stage, the above microstructured fiber provides an ultrawide (over an octave), very smooth and coherent SC when pumped with parameters corresponding to commercially available Er-doped femtosecond fiber lasers.

2. Dispersion design

The first step consists in exploring the possibilities to engineer the GVD in PCFs made up of soft glass. We have paid attention to the Schoot SF57 glass [14]. This commercial lead-silicate glass exhibits very high nonlinearity and was already employed in the fabrication of complex PCF preforms showing up to 160 air holes [11]. The dispersive properties of SF57 glass are significantly different to that shown by fused silica. In fact in Fig. 1 the solid curve shows the GVD coefficient, β_2, corresponding to bulk SF57 glass. We point out that the intrinsic ZDW is around 1.97 μm and $\beta_2 \approx 66\,\mathrm{ps}^2/\mathrm{km}$ at 1.55 μm (we recall that the same values for fused silica are $\lambda \approx 1.3\,\mu\mathrm{m}$ and $\beta_2 \approx -28\,\mathrm{ps}^2/\mathrm{km}$). In addition, SF57 glass shows a higher refractive index than fused silica (1.81 against 1.44, both at 1.55 μm), leading to a higher waveguide-dispersion contribution.

It is a challenge to search for soft-glass PCF geometric parameters to achieve an ultraflattened dispersion profile in the region around 1.55 μm. To this end, we first adapted the design procedure established in [4] to the current case and have used our own numerical algorithm [15] to evaluate both β_2 and the effective mode area as a function of the frequency, $A_{eff}(\omega)$. In this way, for an equally-sized, air-hole soft-glass PCF, the best flattened dispersion profile we achieved is shown in Fig. 1 (short-dashed curve). The pitch and the radius of the holes of the above triangular PCF, denoted as fiber #1, are $\Lambda = 1.7\,\mu\mathrm{m}$ and $a = 0.29\,\mu\mathrm{m}$, respectively. The result is far away to our goal, a positive and nearly constant β_2-profile. In a second phase, we add an additional degree of freedom and consider a triangular soft-glass PCF with two families of air-hole sizes. Then, using our recently developed inverse design technique [16] and starting from the above result, we have reached the impressive ultraflattened dispersion behavior shown in Fig. 1 (long-dashed curve). In this case, the radius of the first inner ring of air holes is $a_1 = 0.20\,\mu\mathrm{m}$, the radius of the rest of holes $a_2 = 0.37\,\mu\mathrm{m}$, and $\Lambda = 1.07\,\mu\mathrm{m}$. It is worth stating at this point that we have selected as target value $\beta_2 \approx 20\,\mathrm{ps}^2/\mathrm{km}$ because it is a good choice to accomplish our next objective. Needless to say that it is possible to achieve a flatter PCF dispersion behavior if we consider a higher number of rings with different sized air-holes. However, we only take into account PCFs relatively simple hole structures as in the above PCF, called fiber #2, to keep up the feasibility of their fabrication.

3. Nonlinear propagation and SC generation

Our second goal is the generation of an ultrawide and very smooth SC. To this end, nonlinear propagation along the z-axis of the fiber is evaluated by integrating in a conventional way the generalized nonlinear Schrödinger propagation equation, expressed as [17]

$$\frac{\partial A(z,T)}{\partial z} = \sum_{n\geq 2} \frac{i^{n+1}}{n!}\beta_n \frac{\partial^n A}{\partial T^n} + i\left(\gamma_0 + i\gamma_1 \frac{\partial}{\partial T} - \frac{\gamma_2}{2}\frac{\partial^2}{\partial T^2}\right)\left(A(z,T)\int_{-\infty}^{T} R(T')\left|A(z,T-T')\right|^2 dT'\right), \tag{1}$$

#107640 - $15.00 USD Received 18 Feb 2009; revised 3 Apr 2009; accepted 3 Apr 2009; published 15 May 2009

where $A(z,T)$ is the optical field envelope, T denotes the proper time, and β_n and γ_n are the nth derivative of the propagation constant, $\beta(\omega)$, and the nonlinear coefficient, $\gamma(\omega) = n_2\omega/cA_{eff}(\omega)$, respectively, with respect to ω evaluated at the carrier frequency. The nonlinear refractive index of SF57 glass is $n_2 = 4.1\times10^{-19}\ \mathrm{m^2/W}$ [18], around 15 times larger than that of the fused silica, and we stress that the frequency dependence of the effective mode area is considered in our numerical calculations. The nonlinear response function, $R(T) = (1-f_R)\delta(T) + f_R h_R(T)$, includes both instantaneous electronic and delayed Raman contributions. The first term of the right-hand part in Eq. (1) describes the whole dispersion effects. In fact, we have taken into account the entire dispersion operator by performing in the frequency domain the multiplication of the complex spectral envelope, $\tilde{A}(z,\omega)$, by the quantity $\beta(\omega) - \omega\beta_1 - \beta_0$. The second term of the right-hand side models nonlinear effects, such as self-phase modulation (SPM), self-steepening, formation of shock waves, and stimulated Raman scattering. In our simulations, $f_R = 0.1$ and the Raman response function, $h_R(T)$, of the SF57 glass is described by means of an analytic form based on experimental measurements [18]. Note that we have neglected linear losses since the propagation distance is only a few centimeters for all cases. Finally, we assumed a hyperbolic-secant input pulse emerging form a Femtolite Ultra Bx-60 laser with $\lambda = 1550$ nm, average power $P_{av} = 60\,\mathrm{mW}$, pulse width $T_0 = 100$ fs, and repetition rate $f = 50$ Mhz.

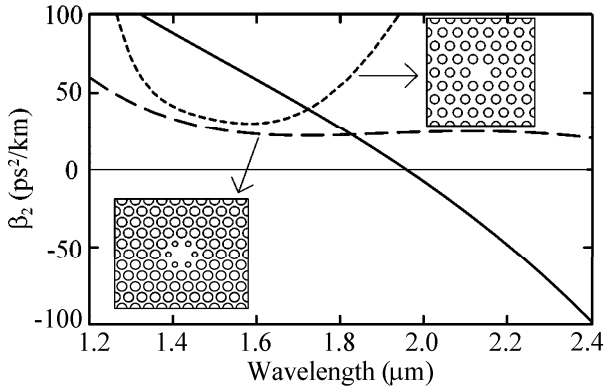

Fig. 1. GVD coefficient vs wavelength for both bulk SF57 glass (solid curve) and two SF57-glass PCF configurations (dashed curves). Insets sketch the unlimited structures under consideration.

It is interesting to keep in mind that in the normal dispersion regime the spectral broadening factor for femtosecond pulses is given by $N = \sqrt{\gamma P_0 T_0^2/\beta_2}$ [19]. In Fig. 2 we present some numerical simulations showing the spectral evolution of the pulsed light traveling through fibers #1 and #2 for three selected propagation lengths. At initial distances we point out that SPM chiefly produces the rapid expansion of the spectrum. At this first stage, we may recognize that the typical deep oscillations in the spectral profile produced by SPM result from the interference between temporally shifted spectral components. On the other hand, the spectral asymmetric behavior is a consequence of self-steepening. As the pulse propagates the spectral modulation gradually decreases due to dispersion, but self-steepening simultaneously stresses dispersion effects, preventing spectral broadening.

#107640 - $15.00 USD Received 18 Feb 2009; revised 3 Apr 2009; accepted 3 Apr 2009; published 15 May 2009

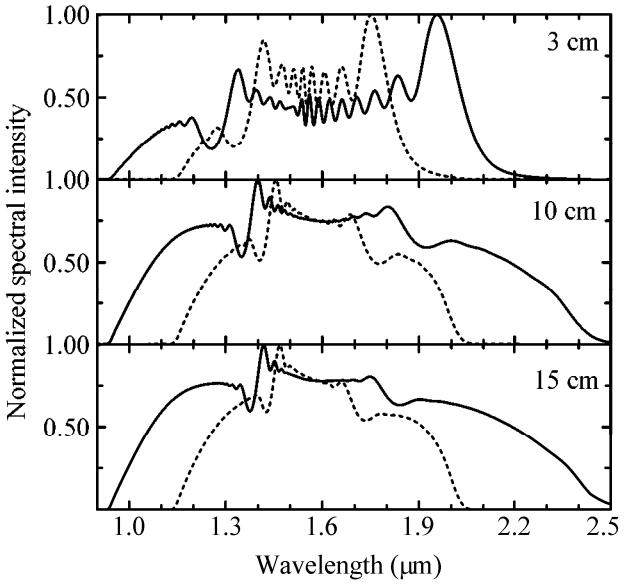

Fig. 2. Normalized spectral intensity vs wavelength for three propagation distances. Solid curves correspond to fiber #2 and broken curves to fiber #1.

In this case, it appears that a 10-cm fiber #2 length is enough to attain the wanted profile. In fact, the region of interest is slightly narrower, although more flattened, after 15-cm propagation. After inspection of Fig. 2, the conclusion is clear. The SC generated with fiber #2 is broader and very flat and the explanation is simple. The SC is very flat since fiber #2 shows an ultraflattened dispersion curve, as would be expected. Likewise, the greater the broadening factor N, the wider the SC. This assessment applies to fiber #2 due to two reasons. The first one is that, β_2-coefficient is rather smaller than that of fiber #1. The second one, and more important, is that the nonlinear coefficient γ is around 2.5 times bigger. We gather the above statement when we compare the pitch value of fibers #2 and #1, which finally determine the effective mode area, A_{eff}, of the corresponding guided modes. In other words, fiber #2 shows two key features, a more flattened dispersion and a greater nonlinear coefficient compared with fiber #1.

4. SC flatness

Note that the scale of the spectral intensity in Fig. 2 is linear. In logarithmic scale, we recognize an ultraflat SC spectrum with deviations less than 3 dB over an octave (see solid curve in Fig. 3). In order to put this result in context, we would like to emphasize that experimental octave-spanning SC generation in soft-glass PCFs was already reported [13, 20]. However in both experiments the SC presents fluctuations around 20 dB. A qualitatively different attempt using a fused-silica PCF was also reported [21]. In this last case, the oscillations approximately reach 10 dB. We claim that the key point to attain our objective was the design of the fiber geometry in order to reach a low, positive and ultraflat dispersion shape. In principle, we expect that this behavior must be very robust against variations of the input pulse characteristics. In order to verify this high stability, we have calculated the output power spectrum for fairly large peak power fluctuations ($\pm 4\%$) of the incoming pulse. The results are illustrated in Fig. 3. We realize that the three curves overlap in the region of interest. Of course, our numerical simulations do not include dispersion variations resulting from imperfections of material properties and manufacture, as well as attenuation. In this sense, our results are ideal in comparison to experimental verifications.

#107640 - $15.00 USD Received 18 Feb 2009; revised 3 Apr 2009; accepted 3 Apr 2009; published 15 May 2009

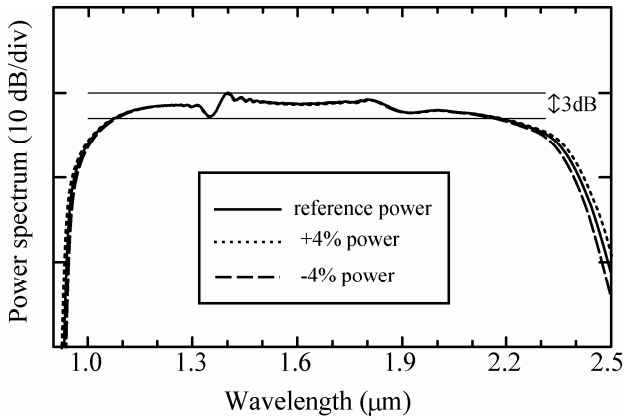

Fig. 3. Output power spectrum vs wavelength after 10-cm propagation throughout fiber #2 for three different peak powers of the incident pulse.

Going one step further, we compared the output spectrum for three different commercial Er-doped femtosecond fiber lasers, the Femtolite Ultra Bx-60, the CF1560-HP ($\lambda = 1550$ nm, $P_{av} = 130\text{mW}$, $T_0 = 90$ fs, and $f = 100$ Mhz) and the Buccaneer ($\lambda = 1550$ nm, $P_{av} = 100\text{mW}$, $T_0 = 250$ fs, and $f = 70$ Mhz) after 15-cm propagation in fiber #2. The numerical results in dB are shown in Fig. 4. It is clear that the output peak-power level is different in each case.

Note that in the present work we focus our attention on the flatness and wideness of the emerging SC, not in its power density level. We stress that these characteristics are still preserved, even for different lasers, when we deal with $\beta_2 > 0$. This is the last reason why we do not consider insertion losses. We would certainly be able to get better results if the dispersion profile is specifically adapted to each laser system with its corresponding coupling efficiency. This discussion reveals once more the central role that the GVD design plays in the SC generation.

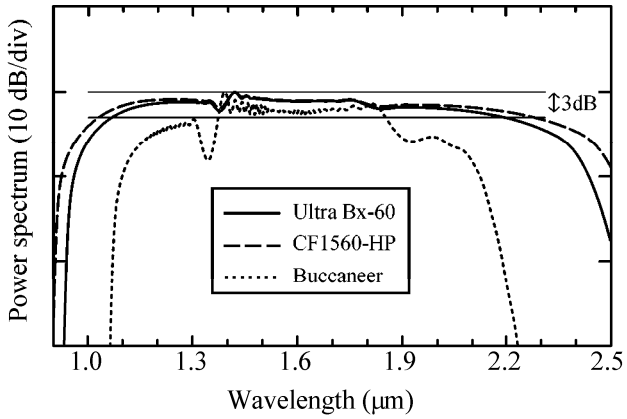

Fig. 4. Output power spectrum vs wavelength after 15-cm propagation throughout fiber #2 for three different commercial femtosecond lasers.

5. Conclusion

Our main claim is to highlight the possibility of finding ultraflat dispersion designs dealing with easy-to-fabricate soft-glass PCFs. Due to the inherent high nonlinearity of the material, the above fibers are well-adapted to produce octave-spanning ultraflat SC with different pumping femtosecond lasers, when operating at the fiber normal dispersion regime.

#107640 - $15.00 USD Received 18 Feb 2009; revised 3 Apr 2009; accepted 3 Apr 2009; published 15 May 2009

Acknowledgments

This work was funded by the Ministerio de Ciencia e Innovación, Spain (grant TEC2008-05490). Partial financial support by the Generalitat Valenciana, Spain (grant GV/2007/043), is also acknowledged.

#107640 - $15.00 USD Received 18 Feb 2009; revised 3 Apr 2009; accepted 3 Apr 2009; published 15 May 2009